


**Light-Emitting Diodes** Hot Paper
How to cite: *Angew. Chem. Int. Ed.* **2021**, *60*, 8337–8343

International Edition: doi.org/10.1002/anie.202100243

German Edition: doi.org/10.1002/ange.202100243

# Highly Efficient Halide Perovskite Light-Emitting Diodes via Molecular Passivation

 Aihui Liang<sup>+</sup>, Kang Wang<sup>+</sup>, Yao Gao, Blake P. Finkenauer, Chenhui Zhu, Linrui Jin, Libai Huang, and Letian Dou\*

**Abstract:** Metal halide perovskites are promising for applications in light-emitting diodes (LEDs), but still suffer from defects-mediated nonradiative losses, which represent a major efficiency-limiting factor in perovskite-based LEDs (PeLEDs). Reported here is a strategy to synthesize molecular passivators with different anchoring groups for defects passivation. The passivated perovskite thin films exhibit improved optoelectronic properties as well as reduced grain size and surface roughness, thus enable highly efficient PeLEDs with an external quantum efficiency of 15.6% using an imidazolium terminated passivator. Further demonstrated is that the *in situ* formation of low-dimensional perovskite phase on the surface of three-dimensional perovskite nanograins is responsible for surface defects passivation, which leads to significantly enhanced device performance. Our results provide new fundamental insights into the role of organic molecular passivators in boosting the performance of PeLEDs.

## Introduction

Metal halide perovskites (MHPs) are emerging as a new class of semiconducting materials with many remarkable optoelectronic properties such as facile solution processability,<sup>[1]</sup> tunable band gap,<sup>[2]</sup> balanced charge transport properties with long diffusion lengths,<sup>[3]</sup> and high photoluminescence quantum yield (PLQY),<sup>[4]</sup> which have attracted considerable interests in optoelectronic applications, such as solar cells,<sup>[5]</sup>

light-emitting devices,<sup>[6]</sup> photodetectors<sup>[7]</sup> and field-effect transistors.<sup>[8]</sup> Particularly, owing to the high color purity with narrow spectra emission (full-width at half-maximum (FWHM)  $\leq 20$  nm),<sup>[9]</sup> and broad range of color tunability (400–1000 nm),<sup>[10]</sup> MHPs are widely used in light-emitting diodes. In 2014, Tan et al. first reported the perovskite light-emitting diodes (PeLEDs) using three-dimensional (3D) perovskite  $\text{CH}_3\text{NH}_3\text{PbI}_3$  (MAPbI<sub>3</sub>) and  $\text{CH}_3\text{NH}_3\text{PbBr}_3$  (MAPbBr<sub>3</sub>) as emitting layers, which showed an external quantum efficiency (EQE) of 0.76% and 0.1%, respectively.<sup>[6a]</sup> Since then, the EQE of PeLEDs has been boosted to over 20% by adopting two different approaches.<sup>[11]</sup> One way is to enhance radiative recombination rates by confining the electrons and holes, which include the use of ultra-thin emissive layers,<sup>[12]</sup> the fabrication of nanoscale polycrystalline features,<sup>[13]</sup> the design of low-dimensional or multiple quantum well structures,<sup>[14]</sup> and the synthesis of perovskite quantum dots.<sup>[15]</sup> The other way is to suppress the defects-related nonradiative recombination, which have been identified as a major efficiency-limiting factor for PeLEDs.<sup>[16]</sup>

In fact, the state-of-the-art solution-processed perovskite materials suffer from severe defect-mediated nonradiative losses, which are generally believed to be associated with ionic defects, such as lead vacancies and halide vacancies.<sup>[17]</sup> At the same time, the ionic nature of the perovskite lattice enables molecular passivation through coordinate binding based on Lewis acid-base chemistry.<sup>[18]</sup> Organic molecules with different functional groups have been employed as molecular passivators to passivate perovskite surface defects.<sup>[18a,19]</sup> For instance, in 2017, Xiao et al. incorporated large-group *n*-butylammonium halides (BAX, X = I, Br) into the perovskite precursor solution acting as a surfactant that dramatically constrains the growth of 3D perovskite grains and decreases film roughness, which increased the EQE of MAPbI<sub>3</sub> and MAPbBr<sub>3</sub> based PeLEDs from 1.0% to 10.4% and 0.03% to 9.3%, respectively.<sup>[13]</sup> Later in 2019, several bulky organoammonium ligands such as 4-fluorophenylmethylammonium iodide (4-F-PMAI) and 4,5-fluorophenylmethylammonium iodide (4,5-F-PMAI) were used, and a highly efficient MAPbI<sub>3</sub>-based PeLEDs with EQE  $\approx 15\%$  was achieved.<sup>[20]</sup> However, most of the currently used passivators are based on primary ammonium terminated molecules, which still suffer from limited device efficiency and stability, and there is a lack of deep understanding of how the molecules interact with the perovskites.

In this work, we synthesized a series of new phenyl and thienyl-based molecular passivators with ammonium, formamidinium and imidazolium terminal groups, to examine the

[\*] Dr. A. Liang<sup>[†]</sup>College of Chemistry and Chemical Engineering, Jiangxi Normal University  
Nanchang, 330022 (P. R. China)Dr. A. Liang,<sup>[†]</sup> Dr. K. Wang,<sup>[†]</sup> Dr. Y. Gao, B. P. Finkenauer, Prof. L. Dou  
Davidson School of Chemical Engineering, Purdue University  
West Lafayette, IN 47907 (USA)  
E-mail: dou10@purdue.eduProf. C. Zhu  
Advanced Light Source, Lawrence Berkeley National Laboratory  
Berkeley, CA 94720 (USA)L. Jin, Prof. L. Huang  
Department of Chemistry, Purdue University  
West Lafayette, IN 47907 (USA)Prof. L. Dou  
Birck Nanotechnology Center, Purdue University  
West Lafayette, IN (USA)

[†] These authors contributed equally to this work.

 Supporting information and the ORCID identification number(s) for the author(s) of this article can be found under:  
 <https://doi.org/10.1002/anie.202100243>.

effects of different anchoring groups on defect passivation. After introducing the passivators, the as-prepared perovskite thin films display improved optoelectronic properties with low nonradiative recombination rate and high PLQY as well as reduced grain size and surface roughness. On this basis, we demonstrate highly efficient PeLEDs with an EQE of 15.6% using a novel imidazolium terminated passivator. Employing grazing incidence wide-angle X-ray scattering technique and single-crystal analysis, we further confirm that the in situ formation of low-dimensional perovskite phase on the surface of 3D perovskite nanograins is responsible for the surface defects passivation, which lead to significantly enhanced device performances. Our results suggest imidazolium can serve as highly efficient passivation group for high-performance PeLEDs.

## Results and Discussion

We fabricated the PeLEDs based on a device structure of ITO/Poly-TPD/perovskite/TPBi/LiF/Al (Figure 1a) with energy diagrams shown in Figure 1b. Poly[N,N'-bis(4-butylphenyl)-N,N'-bis(phenyl)-benzidine] (Poly-TPD) was used as the hole-transporting layer, 1,3,5-tris(1-phenyl-1*H*-benzimidazol-2-yl)benzene (TPBi) was used as the electron-transporting layer, 3D organic-inorganic hybrid perovskite (MAPbI<sub>3</sub>) was used as the emitting layer, and indium tin oxide (ITO) and LiF/Al were used as the anode and cathode, respectively. Besides those conventional ammonium tails, formamidinium and imidazolium also can anchor to the Pb-I framework through coordination with the Pb ions or hydrogen bonding with the iodide ions.<sup>[21]</sup> Moreover, benzene and thiophene rings are hydrophobic and their  $\pi$ -conjugation structure favors charge transport. Organic molecules with phenyl or certain thienyl substituents exhibited very different anchoring interactions and passivation effects with perovskites.<sup>[22]</sup> Hence, we introduced several phenyl and thienyl-based bulky molecular passivators with different anchoring tails (methylammonium (MA<sup>+</sup>), formamidinium (FA<sup>+</sup>) and

imidazolium (Im<sup>+</sup>)) to passivate the potential surface defects of MAPbI<sub>3</sub> films. The molecular structures of these passivators are shown in the right panel in Figure 1a, where phenylmethylammonium iodide (PMAI) and thienylmethylammonium iodide (TMAI) were purchased from commercial sources. The other passivators, including phenylformamidinium iodide (PFAI), thienylformamidinium iodide (TFAI), phenylimidazolium iodide (PImI) and thienylimidazolium iodide (TImI) are synthesized in our lab and their synthetic routes are shown in the Methods section found in the Supporting Information. PFAI and TFAI were prepared from benzonitrile and thiophene-2-carbonitrile, respectively. The nitrile is reacted with sodium methoxide in methanol followed by treatment with acetic acid and ammonium chloride, and then treated with aqueous hydrogen iodide to give the desired molecules. PImI and TImI were obtained by using aqueous hydrogen iodide to deprotect tert-butyl 4-phenyl-1*H*-imidazole-1-carboxylate and tert-butyl 4-(thiophen-2-yl)-1*H*-imidazole-1-carboxylate, which were synthesized from phenylboronic acids and tributyl(thiophen-2-yl)stannane reacted with tert-butyl 4-bromo-1*H*-imidazole-1-carboxylate by Suzuki–Miyaura and Stille cross-coupling reactions, respectively. All the chemical structures of the target passivators were identified by <sup>1</sup>H and <sup>13</sup>C nuclear magnetic resonance (NMR) spectroscopy and mass spectrometry (MS).

In order to find the optimal molar ratio of molecular passivators, we primarily sought to fabricate the PeLEDs by introducing different amounts of PMAI into MAPbI<sub>3</sub> precursor solutions. As displayed in Figure S1 in the Supporting Information, the EQE of the PeLEDs shows an increasing trend when the molar ratio of PMAI increased from 5% to 20%, while further increasing the molar ratio to 30% results in an EQE decrease. All these results are consistent with previous works.<sup>[13,20]</sup> As a result, we set the molar ratio of all the molecular passivators at 20% for further spectroscopic and morphologic studies. The absorption and photoluminescence (PL) spectra of perovskite films with different passivators (PMAI, PFAI, PImI, TMAI, TFAI, and TImI) at the molar ratios of 20% are shown in Figure 2a and b. Relative to

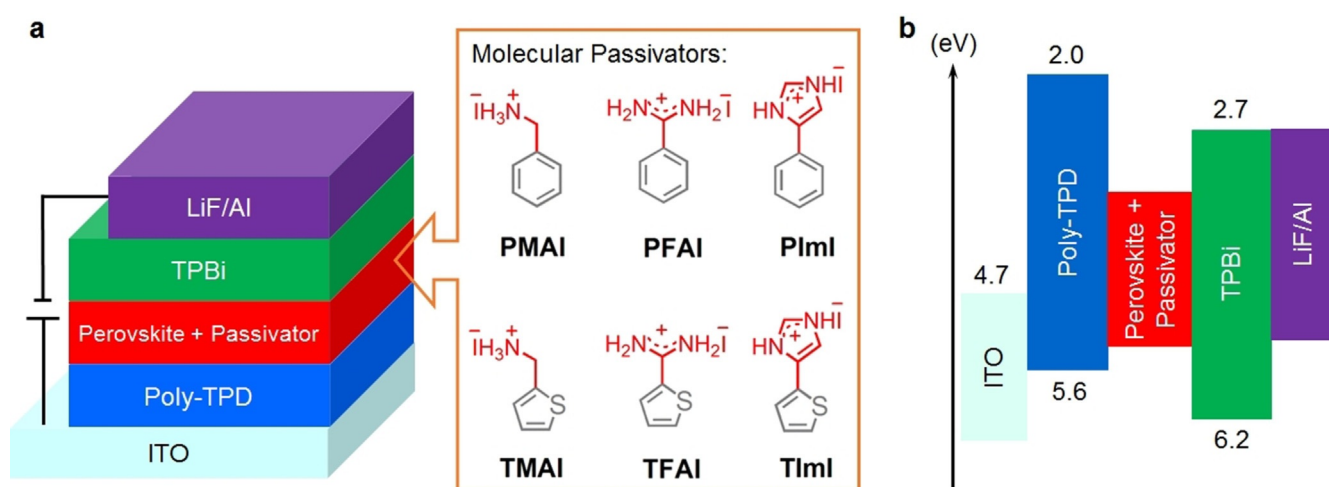


**Figure 1.** a) Device structure of the PeLEDs. The library of molecular passivators with different terminal groups and conjugated heads is shown on the right. b) Energy level diagrams of MAPbI<sub>3</sub>-based PeLEDs. The energy levels of the perovskite and other layers are taken from literature.

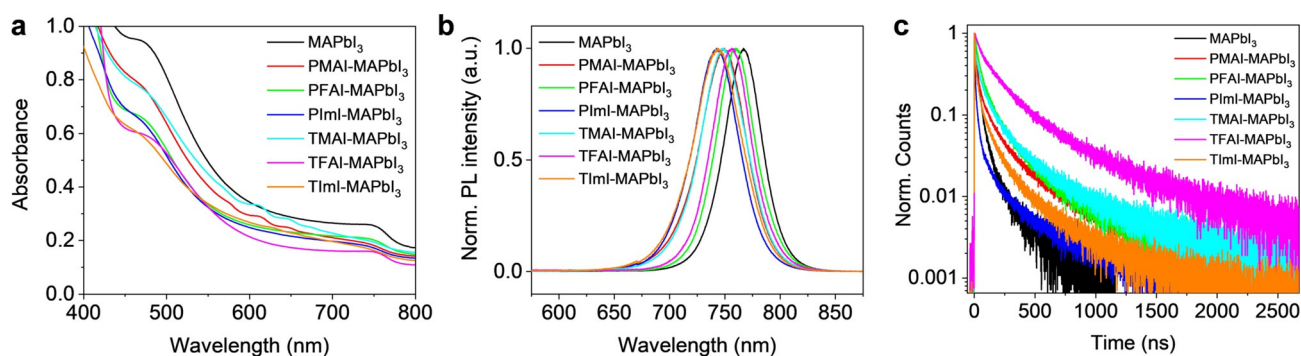


**Figure 2.** a) Absorption, b) PL spectra, and c) TRPL lifetime of MAPbI<sub>3</sub> thin films with or without 20% molar excess of different passivators in the precursor solutions.

that of the control MAPbI<sub>3</sub> film without passivators, the absorption edges and PL peaks of passivated perovskite films exhibit a small blue-shift, which could be corresponding to the emergence of low-dimensional perovskite grains and the reduction in crystallite size, thus increasing the band energy by quantum confinement effect.<sup>[13]</sup> The PLQY and time-resolved photoluminescence (TRPL) were then conducted on these perovskite films to examine their carrier recombination dynamics. As shown in Table S1 in the Supporting Information, the PLQY of the perovskite films with passivators are dramatically increased compared with the control MAPbI<sub>3</sub> film. Specifically, passivators with phenyl group show higher PLQY than the corresponding passivators with thienyl group. This should be attributed to the existence of heavy sulfur atom in thienyl-based molecules and the efficient solid-state packing characteristic, which will limit the fluorescent quantum yields in both solution and the solid state.<sup>[23]</sup>

Based on the TRPL curves, the average lifetime ( $\tau_{av}$ ) of the control MAPbI<sub>3</sub> film is fitted to be 47.5 ns (Figure 2c and Table S1, Supporting Information). In contrast, the perovskite films with the passivators exhibited longer average carrier lifetimes, which implies that defect-assisted non-radiative processes are effectively suppressed.<sup>[4a]</sup> Accordingly, the radiative and nonradiative recombination rate ( $k_r$  and  $k_{nr}$ ) of those perovskite films were calculated using the expressions  $PLQY = k_r / (k_r + k_{nr})$  and  $\tau_{av} = (k_r + k_{nr})^{-1}$ . The results are summarized in Table S1 in the Supporting Information. In comparison with the control MAPbI<sub>3</sub> film, the perovskite film with the passivators showed a smaller  $k_{nr}$ , which further confirms the passivation effects of the as-obtained molecular passivators. As shown in Table S1, the perovskite films with phenyl-based passivators showed higher  $k_r$  than the corresponding perovskite films with thienyl-based passivators. Furthermore, the film containing 20% molar excess PImI yielded the highest  $k_r$  ( $21.3 \times 10^5 \text{ s}^{-1}$ ), suggesting that the PLQY improvement was primarily due to enhanced radiative decay processes. Interestingly, both phenyl and thienyl group based passivators with different tails exhibit the  $k_r$  in the order of  $\text{Im}^+ > \text{MA}^+ > \text{FA}^+$ , which suggest varied passivation effect of different terminal groups. Such enhanced radiative recombination together with suppressed non-radiative recombination makes PImI the most promising passivator for high-performance PeLEDs.

Notably, these phenyl- and thienyl-based passivators with different terminal group are too large to fit into the corner of  $[\text{PbI}_6]^{4-}$  octahedral layers due to the restriction of tolerance factor, and therefore induce the formation of low-dimensional perovskite phase, which will impede the growth of 3D perovskite grains during the film formation process. To investigate the influence of the chemical structure of organic molecular passivators on film morphology, we further conduct atomic force microscope (AFM) measurements. Compared to the control MAPbI<sub>3</sub> film, the crystallite size and the film root mean square roughness (r.m.s) were significantly reduced when adding the passivators (PMAI, TMAI, PImI and TImI) into the perovskite films. However, the r.m.s is a little larger while PFAI and TFAI were added into the perovskite films (Figure 3a–g). The PImI passivated MAPbI<sub>3</sub> film (Figure 3d) is the most uniform and smooth one with a r.m.s. of  $\approx 1.14$  nm, which is among the most flat and uniform perovskite films reported so far.<sup>[13,24]</sup> The same influence of grain size and smooth surface of the perovskite film after incorporating of passivators can also be visualized by scanning electron microscopy (SEM) (Figure S2, Supporting Information). The smaller perovskite grain size can increase the exciton binding energy to improve the PLQY, and the reduced surface roughness can help decrease the trap density and avoid current leakage, both of which are favorable for LED applications.

Figure S3–S7 present the device performances of PeLEDs with different molecular passivators (PFAI, PImI, TMAI, TFAI, and TImI) as the molar ratio increased from 5% to 30%. The optimal molar ratio of all passivators doped in the perovskite layer are determined to be 20%, which are consistent with previous reports.<sup>[13]</sup> The current density–voltage ( $J$ – $V$ ) curves of the champion PeLEDs with different passivators are shown in Figure 4a. The passivated films maintain their current densities at a very low level below 2 V, suggesting negligible current leakage in our PeLED devices. The abrupt increase of current densities after 2 V indicates the injection of charge carrier into perovskite materials. As shown in Figure 4b, the EQEs of PeLEDs with phenyl-based passivators are much higher than the corresponding thienyl-based passivators. More interestingly, the PeLEDs performances of phenyl- or thienyl-based passivators with different tails are in the order of  $\text{Im}^+ > \text{MA}^+ > \text{FA}^+$  (detailed in

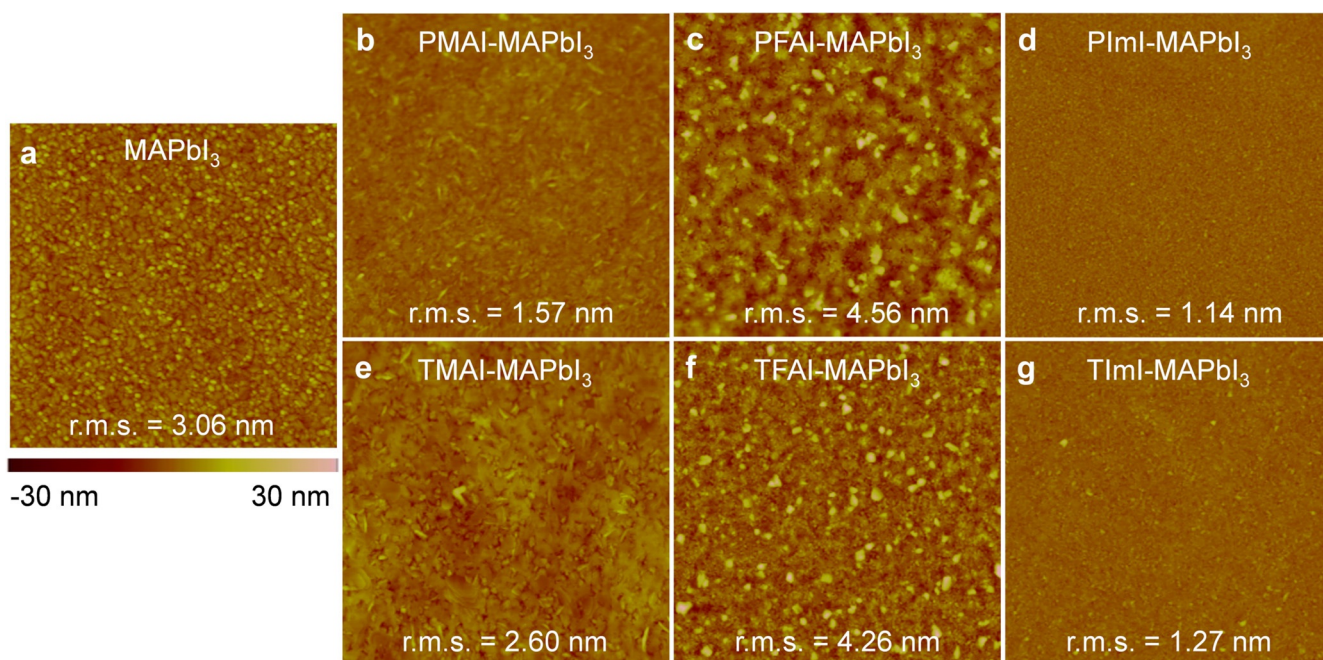


**Figure 3.** AFM height image of MAPbI<sub>3</sub> thin films with or without 20% molar excess of different passivators in the precursor solutions. a) MAPbI<sub>3</sub>; b) PMAI-MAPbI<sub>3</sub>; c) PFAI-MAPbI<sub>3</sub>; d) PlmI-MAPbI<sub>3</sub>; e) TMAI-MAPbI<sub>3</sub>; f) TFAI-MAPbI<sub>3</sub>; g) TImI-MAPbI<sub>3</sub>. The scan area of AFM images is 5  $\mu\text{m} \times 5 \mu\text{m}$ .

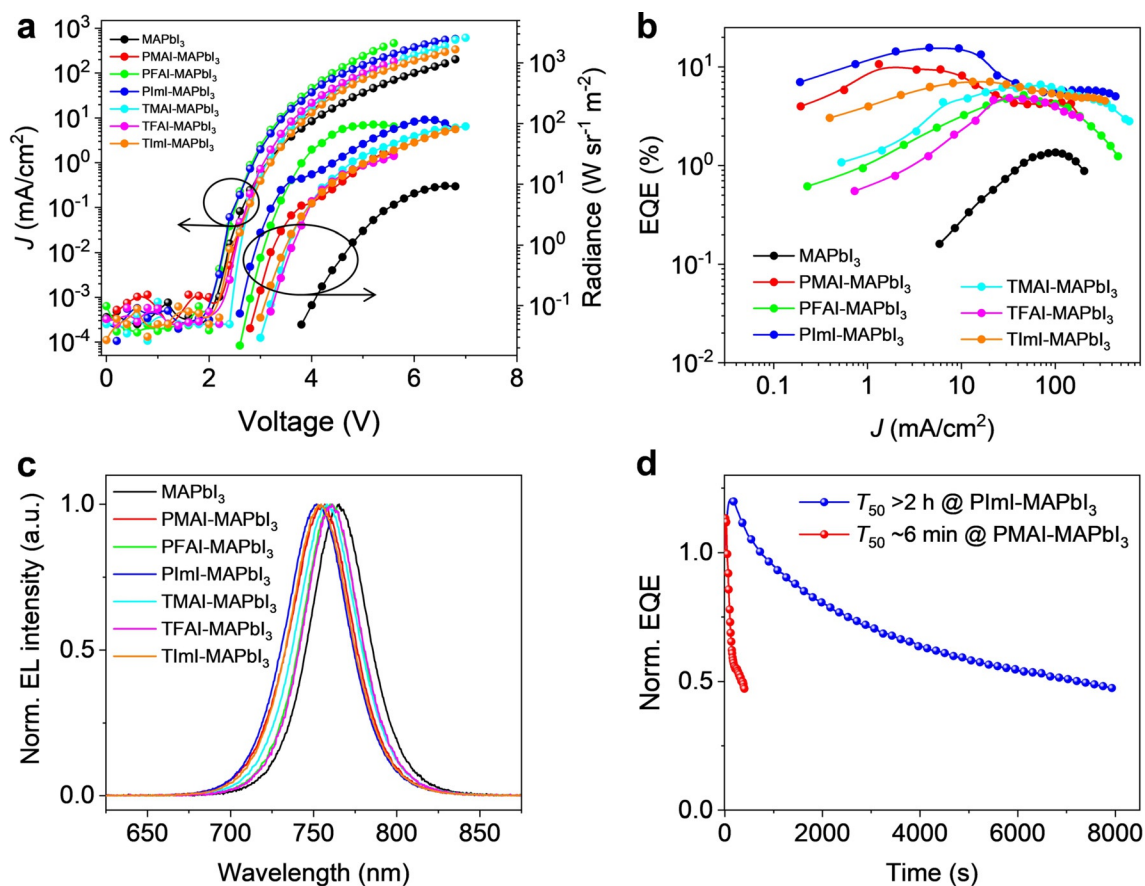


**Figure 4.** a) Current density ( $J$ )-voltage ( $V$ )-radiance ( $R$ ) curves, b) EQE versus current density, and c) normalized EL spectra of PeLEDs with or without 20% molar excess of different molecular passivators. d) Operational stabilities of the device with PMAI and PlmI passivators tested at a constant current density of 10  $\text{mA cm}^{-2}$ .

Table S2, Supporting Information), which is in good agreement with the results of spectroscopy and morphology studies. Most importantly, the device with PImI passivator shows the highest EQE of 15.6%, which is ten-fold higher than that of the control device and among the highest value for MAPbI<sub>3</sub> based PeLEDs (Figure S8 and S9, Supporting Information).

The electroluminescent (EL) peaks of all perovskite devices displayed blue-shift with increasing amounts of molecular passivators. The blue-shift of EL spectra can be attributed to the terminal group of passivators, which results from the change of crystalline structure, film morphology, and the surface trap passivation effect.<sup>[25]</sup> Fortunately, no wavelength shift of EL spectra was observed under different applied bias voltage, indicating good color-stability of the PeLEDs (Figure S3–S7, Supporting Information). Figure 4c plots the normalized EL spectra of PeLEDs with different molecular passivators at a molar ratio of 20%, where EL wavelength is increasingly blue-shifted from MAPbI<sub>3</sub>, FA<sup>+</sup>-passivated, MA<sup>+</sup>-passivated, to Im<sup>+</sup>-passivated PeLEDs. This can be ascribed to the decreased grain size. In addition to the remarkably enhanced device efficiency, the PeLEDs based on the PImI passivator also exhibit considerably better operational stability. The EQE of the PImI-based device dropped to half of the initial value after 2 h under a constant current density of 10 mA cm<sup>-2</sup> (Figure 4d). This result demonstrates that the stability of PImI-based device is significantly improved even compared with the PMAI-based device, which can only survive for about 6 minutes under the same conditions. All of these results suggest that the LED device performances regarding EQE and EL wavelengths are strongly related to the terminal anchoring group of those molecular passivators.

In order to determine the origin of the EQE enhancement with PImI and further understand the interaction of molecular passivators with perovskites, we carried out crystallo-

graphic studies with thin film X-ray diffraction (XRD), two-dimensional synchrotron-based grazing incidence wide-angle X-ray scattering (GIWAXS), and single-crystal analysis. As shown in Figure 5a, the passivated MAPbI<sub>3</sub> films exhibit similar XRD spectra with two diffraction peaks around 14° and 28°, corresponding to (110) and (220) planes of 3D perovskite, respectively.<sup>[26]</sup> No diffraction peaks corresponding to low-dimensional perovskites are clearly observed after the introduction of molecular passivators, which indicate that the as-formed films with passivators are nearly indistinguishable from the control 3D perovskite crystal structure. However, those XRD peaks become broad after adding the passivators into the perovskite film. According to Scherrer Equation (1),<sup>[27]</sup> the larger FWHM corresponds to a smaller average crystallite size.

$$L = \frac{0.9\lambda}{\Delta_{2\theta}\cos\theta} \quad (1)$$

where  $L$  is the mean size of the perovskite crystalline domains,  $\lambda$  is the wavelength of incident X-ray,  $\Delta_{2\theta}$  is the full width at half maximum of the peak, and  $\theta$  is the Bragg angle. After adding passivators, the grain size decreased from  $\approx 46$  nm for MAPbI<sub>3</sub> to 15 nm for PImI-MAPbI<sub>3</sub> (see Table S1, Supporting Information for more details), which is consistent with the SEM and AFM results.

The recorded GIWAXS patterns of the control and of the excess passivators incorporated MAPbI<sub>3</sub> perovskite films are shown in Figure 5b–h. The control MAPbI<sub>3</sub> film exhibits nearly isotropic Bragg rings at  $q = 1.0, 1.4, 1.65, 1.7,$  and  $2.0 \text{ \AA}^{-1}$  corresponding to the (110), (112), (211), (202), and (220) crystal planes of 3D perovskite phase (Figure 5b), indicating a random crystallite orientation.<sup>[28]</sup> With passivators, the diffraction patterns appear in the  $q < 1.0 \text{ \AA}^{-1}$  range, which implies the formation of low-dimensional perovskite

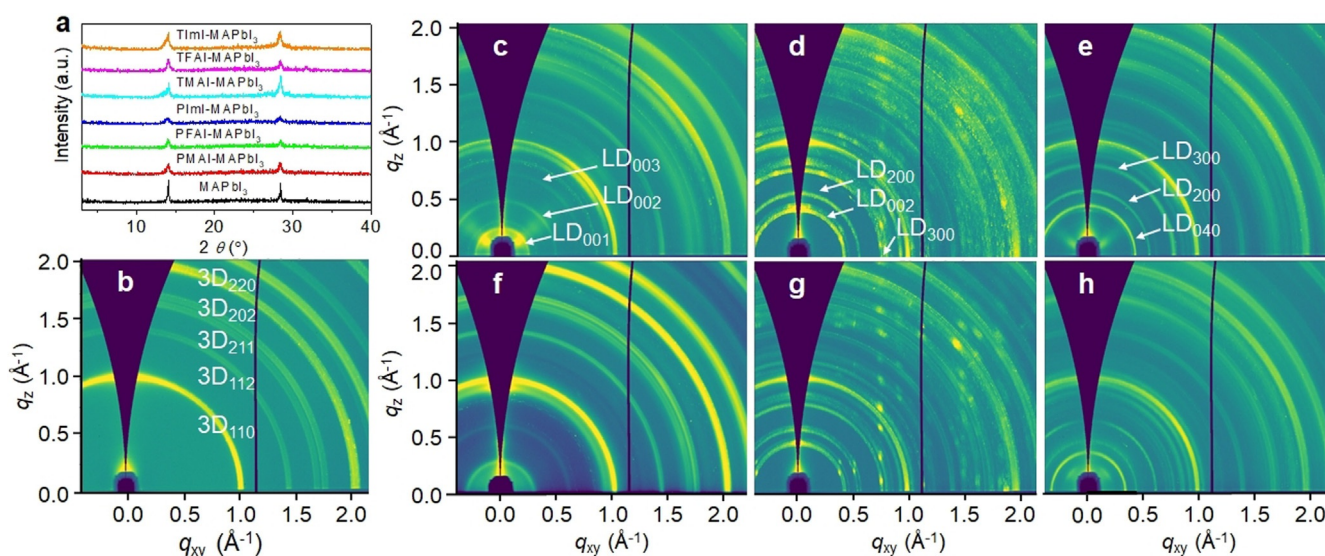


**Figure 5.** a) XRD profile, and b–h) GIWAXS pattern of perovskite thin films with or without 20% molar excess of different passivators for b) MAPbI<sub>3</sub>, c) PMAI-MAPbI<sub>3</sub>, d) PFAI-MAPbI<sub>3</sub>, e) PImI-MAPbI<sub>3</sub>, f) TMAI-MAPbI<sub>3</sub>, g) TFAI-MAPbI<sub>3</sub>, h) TImI-MAPbI<sub>3</sub>. The Miller indices of prominent diffraction peaks are marked in each pattern. The color scale is proportional to the intensity of X-ray scattering. LD, low-dimensional perovskite phase.

structures (Figure 5 c–h).<sup>[28a]</sup> For those PMAI, TMAI, PImI or TImI passivated MAPbI<sub>3</sub> films, the diffraction rings in the  $q < 1.0 \text{ \AA}^{-1}$  can be indexed into different crystal planes of their corresponding low-dimensional perovskite structures (See their single crystal structures in Figure S10, S11, and Table S3, Supporting Information), which have been marked in Figure 5 c, e, f, and h, respectively. Such random orientations and the absence of low-dimension diffraction in thin film XRD pattern indicate the in situ formation of low-dimensional perovskite phase on the surface of 3D perovskite nanograins, which can passivate the surface defects of perovskite and also protect 3D perovskites from being damaged easily, thus leading to enhanced device efficiency and stability. Meanwhile, those resulting low-dimensional perovskites from PMAI and PImI both exhibit that Pb-I bond lengths are around 3.21 Å, while I-Pb-I bond angle is about 158° for PMAI and 90° for PImI, which makes PImI-based low-dimensional perovskites share more similar lattice parameters to those of MAPbI<sub>3</sub> single crystals (Pb-I bond length 3.16 Å, I-Pb-I angle 90°).<sup>[29]</sup> This means that the formation of mixed-phase perovskite nanograins from PImI passivation should have smaller lattice strain than that in PMAI case. Therefore, it is more favorable to passivate the defects and reduce non-radiative loss.<sup>[30]</sup> For PFAI and TFAI (Figure 5 d and g), the perovskite films exhibit a distinct orientation in the direction perpendicular to the substrate and some periodic diffraction spots derived from the low-dimensional perovskites (See its single crystal structures in Figure S12 and Table S3, Supporting Information). In this case, PFAI and TFAI no longer play the role of surface passivator and crystallite terminator, but rather participate in crystallization, which was detrimental to the morphology of our perovskite films (also see SEM and AFM results), and thus could reduce device performances.<sup>[20]</sup>

## Conclusion

In summary, we have synthesized a series of phenyl and thienyl-based molecular passivators with different anchoring groups, such as methylammonium, formamidinium and imidazolium, for defects passivation. The passivators are favorable to passivate the surface defects of perovskites, which led to improved optoelectronic properties regarding suppressed nonradiative losses and enhanced radiative recombination. Morphology studies reveal that those molecular passivators can impede the growth of 3D perovskite nanograins during the film crystallization process, which result in smaller grain size and reduced roughness of the perovskite films. On this basis, we fabricated highly efficient PeLEDs with an EQE of 15.6% using an imidazolium terminated passivator, which are among the best MAPbI<sub>3</sub>-based LEDs reported so far. Further by employing grazing incidence wide-angle X-ray scattering technique and single-crystal analysis, we clearly demonstrated that the in situ formation of mixed-phase perovskite nanograins is possibly responsible for the surface defects passivation, thus leading to significantly enhanced device performances. This work not only provides us a deep insight into the interaction of organic molecules with perovskite lattice for

defects passivation, but also guides the beginning of a new realm of molecular engineering for the development of high-performance perovskite-based optoelectronic devices.

## Acknowledgements

This work is supported by Office of Naval Research (Grant No. N00014-19-1-2296, Program Manager: Dr. Joe Parker and Dr. Paul Armistead) and Davidson School of Chemical Engineering of Purdue University. B.P.F. acknowledges support from the Purdue Process Safety & Assurance Center.

## Conflict of interest

The authors declare no conflict of interest.

**Keywords:** light-emitting diodes · mixed-phase nanograins · molecular passivator · organic-inorganic hybrid perovskite · surface engineering

- [1] a) Q. Chen, H. Zhou, Z. Hong, S. Luo, H.-S. Duan, H.-H. Wang, Y. Liu, G. Li, Y. Yang, *J. Am. Chem. Soc.* **2014**, *136*, 622–625; b) Q. Wang, Y. Shao, Q. Dong, Z. Xiao, Y. Yuan, J. Huang, *Energy Environ. Sci.* **2014**, *7*, 2359; c) Y. Gao, E. Shi, S. Deng, S. B. Shiring, J. M. Snaider, C. Liang, B. Yuan, R. Song, S. M. Janke, A. Liebman-Peláez, P. Yoo, M. Zeller, B. W. Boudouris, P. Liao, C. Zhu, V. Blum, Y. Yu, B. M. Savoie, L. Huang, L. Dou, *Nat. Chem.* **2019**, *11*, 1151–1157.
- [2] a) M. D. Smith, B. A. Connor, H. I. Karunadasa, *Chem. Rev.* **2019**, *119*, 3104–3139; b) V. D’Innocenzo, A. R. Srimath Kandada, M. De Bastiani, M. Gandini, A. Petrozza, *J. Am. Chem. Soc.* **2014**, *136*, 17730–17733; c) Z. Chen, C. Zhang, X.-F. Jiang, M. Liu, R. Xia, T. Shi, D. Chen, Q. Xue, Y.-J. Zhao, S. Su, H.-L. Yip, Y. Cao, *Adv. Mater.* **2017**, *29*, 1603157.
- [3] a) S. D. Stranks, G. E. Eperon, G. Grancini, C. Menelaou, M. J. P. Alcocer, T. Leijtens, L. M. Herz, A. Petrozza, H. J. Snaith, *Science* **2013**, *342*, 341–344; b) G. Xing, N. Mathews, S. Sun, S. S. Lim, Y. M. Lam, M. Grätzel, S. Mhaisalkar, T. C. Sum, *Science* **2013**, *342*, 344–347.
- [4] a) B. Zhao, Y. Lian, L. Cui, G. Divitini, G. Kusch, E. Ruggeri, F. Auras, W. Li, D. Yang, B. Zhu, R. A. Oliver, J. L. MacManus-Driscoll, S. D. Stranks, D. Di, R. H. Friend, *Nat. Electron.* **2020**, *3*, 704–710; b) H. Cho, S.-H. Jeong, M.-H. Park, Y.-H. Kim, C. Wolf, C.-L. Lee, J. H. Heo, A. Sadhanala, N. Myoung, S. Yoo, S. H. Im, R. H. Friend, T.-W. Lee, *Science* **2015**, *350*, 1222–1225.
- [5] a) M. Jeong, I. W. Choi, E. M. Go, Y. Cho, M. Kim, B. Lee, S. Jeong, Y. Jo, H. W. Choi, J. Lee, J.-H. Bae, S. K. Kwak, D. S. Kim, C. Yang, *Science* **2020**, *369*, 1615–1620; b) Q. A. Akkerman, M. Gandini, F. Di Stasio, P. Rastogi, F. Palazon, G. Bertoni, J. M. Ball, M. Prato, A. Petrozza, L. Manna, *Nat. Energy* **2016**, *2*, 16194; c) F. Sahli, J. Werner, B. A. Kamino, M. Bräuninger, R. Monnard, B. Paviet-Salomon, L. Barraud, L. Ding, J. J. Diaz Leon, D. Sacchetto, G. Cattaneo, M. Despeisse, M. Boccard, S. Nicolay, Q. Jeangros, B. Niesen, C. Ballif, *Nat. Mater.* **2018**, *17*, 820–826; d) F. Hao, C. C. Stoumpos, D. H. Cao, R. P. H. Chang, M. G. Kanatzidis, *Nat. Photonics* **2014**, *8*, 489–494.
- [6] a) Z.-K. Tan, R. S. Moghaddam, M. L. Lai, P. Docampo, R. Higler, F. Deschler, M. Price, A. Sadhanala, L. M. Pazos, D. Credgington, F. Hanusch, T. Bein, H. J. Snaith, R. H. Friend, *Nat. Nanotechnol.* **2014**, *9*, 687–692; b) K. Lin, J. Xing, L. N. Quan, F. P. G. de Arquer, X. Gong, J. Lu, L. Xie, W. Zhao, D.

- Zhang, C. Yan, W. Li, X. Liu, Y. Lu, J. Kirman, E. H. Sargent, Q. Xiong, Z. Wei, *Nature* **2018**, 562, 245–248; c) Y. Cao, N. Wang, H. Tian, J. Guo, Y. Wei, H. Chen, Y. Miao, W. Zou, K. Pan, Y. He, H. Cao, Y. Ke, M. Xu, Y. Wang, M. Yang, K. Du, Z. Fu, D. Kong, D. Dai, Y. Jin, G. Li, H. Li, Q. Peng, J. Wang, W. Huang, *Nature* **2018**, 562, 249–253; d) K. Wang, Y. Du, J. Liang, J. Zhao, F. F. Xu, X. Liu, C. Zhang, Y. Yan, Y. S. Zhao, *Adv. Mater.* **2020**, 32, 2001999; e) H. Wang, X. Gong, D. Zhao, Y.-B. Zhao, S. Wang, J. Zhang, L. Kong, B. Wei, R. Quintero-Bermudez, O. Voznyy, Y. Shang, Z. Ning, Y. Yan, E. H. Sargent, X. Yang, *Joule* **2020**, 4, 1977–1987.
- [7] a) L. Dou, Y. Yang, J. You, Z. Hong, W.-H. Chang, G. Li, Y. Yang, *Nat. Commun.* **2014**, 5, 5404; b) R. Dong, Y. Fang, J. Chae, J. Dai, Z. Xiao, Q. Dong, Y. Yuan, A. Centrone, X. C. Zeng, J. Huang, *Adv. Mater.* **2015**, 27, 1912–1918; c) C. Li, Y. Ma, Y. Xiao, L. Shen, L. Ding, *InfoMat* **2020**, 2, 1247–1256.
- [8] a) Y. Liang, F. Li, R. Zheng, *Adv. Electron. Mater.* **2020**, 6, 2000137; b) H. Zhu, A. Liu, K. I. Shim, J. Hong, J. W. Han, Y.-Y. Noh, *Adv. Mater.* **2020**, 32, 2002717; c) T. Matsushima, S. Hwang, A. S. D. Sandanayaka, C. Qin, S. Terakawa, T. Fujihara, M. Yahiro, C. Adachi, *Adv. Mater.* **2016**, 28, 10275–10281; d) Y. Gao, Z. Wei, P. Yoo, E. Shi, M. Zeller, C. Zhu, P. Liao, L. Dou, *J. Am. Chem. Soc.* **2019**, 141, 15577–15585; e) I.-H. Park, K. C. Kwon, Z. Zhu, X. Wu, R. Li, Q.-H. Xu, K. P. Loh, *J. Am. Chem. Soc.* **2020**, 142, 18592–18598.
- [9] Y.-H. Kim, H. Cho, T.-W. Lee, *Proc. Natl. Acad. Sci. USA* **2016**, 113, 11694–11702.
- [10] a) C. C. Stoumpos, C. D. Malliakas, M. G. Kanatzidis, *Inorg. Chem.* **2013**, 52, 9019–9038; b) L. Protesescu, S. Yakunin, M. I. Bodnarchuk, F. Krieg, R. Caputo, C. H. Hendon, R. X. Yang, A. Walsh, M. V. Kovalenko, *Nano Lett.* **2015**, 15, 3692–3696.
- [11] a) W. Xu, Q. Hu, S. Bai, C. Bao, Y. Miao, Z. Yuan, T. Borzda, A. J. Barker, E. Tyukalova, Z. Hu, M. Kawecki, H. Wang, Z. Yan, X. Liu, X. Shi, K. Uvdal, M. Fahlman, W. Zhang, M. Duchamp, J.-M. Liu, A. Petrozza, J. Wang, L.-M. Liu, W. Huang, F. Gao, *Nat. Photonics* **2019**, 13, 418–424; b) S. A. Veldhuis, P. P. Boix, N. Yantara, M. Li, T. C. Sum, N. Mathews, S. G. Mhaisalkar, *Adv. Mater.* **2016**, 28, 6804–6834.
- [12] G. Li, Z.-K. Tan, D. Di, M. L. Lai, L. Jiang, J. H.-W. Lim, R. H. Friend, N. C. Greenham, *Nano Lett.* **2015**, 15, 2640–2644.
- [13] Z. Xiao, R. A. Kerner, L. Zhao, N. L. Tran, K. M. Lee, T.-W. Koh, G. D. Scholes, B. P. Rand, *Nat. Photonics* **2017**, 11, 108–115.
- [14] N. Wang, L. Cheng, R. Ge, S. Zhang, Y. Miao, W. Zou, C. Yi, Y. Sun, Y. Cao, R. Yang, Y. Wei, Q. Guo, Y. Ke, M. Yu, Y. Jin, Y. Liu, Q. Ding, D. Di, L. Yang, G. Xing, H. Tian, C. Jin, F. Gao, R. H. Friend, J. Wang, W. Huang, *Nat. Photonics* **2016**, 10, 699–704.
- [15] G. Li, J. Huang, H. Zhu, Y. Li, J.-X. Tang, Y. Jiang, *Chem. Mater.* **2018**, 30, 6099–6107.
- [16] I. L. Braly, D. W. deQuilettes, L. M. Pazos-Outón, S. Burke, M. E. Ziffer, D. S. Ginger, H. W. Hillhouse, *Nat. Photonics* **2018**, 12, 355–361.
- [17] a) S. D. Stranks, *ACS Energy Lett.* **2017**, 2, 1515–1525; b) M. Abdi-Jalebi, Z. Andaji-Garmaroudi, S. Cacovich, C. Stavrakas, B. Philippe, J. M. Richter, M. Alsari, E. P. Booker, E. M. Hutter, A. J. Pearson, S. Lilliu, T. J. Savenije, H. Rensmo, G. Divitini, C. Ducati, R. H. Friend, S. D. Stranks, *Nature* **2018**, 555, 497–501.
- [18] a) R. Wang, J. Xue, K.-L. Wang, Z.-K. Wang, Y. Luo, D. Fenning, G. Xu, S. Nuryyeva, T. Huang, Y. Zhao, J. L. Yang, J. Zhu, M. Wang, S. Tan, I. Yavuz, K. N. Houk, Y. Yang, *Science* **2019**, 366, 1509–1513; b) J.-W. Lee, H.-S. Kim, N.-G. Park, *Acc. Chem. Res.* **2016**, 49, 311–319.
- [19] a) X. Zheng, B. Chen, J. Dai, Y. Fang, Y. Bai, Y. Lin, H. Wei, X. C. Zeng, J. Huang, *Nat. Energy* **2017**, 2, 17102; b) D. W. deQuilettes, S. Koch, S. Burke, R. K. Paranjhi, A. J. Shropshire, M. E. Ziffer, D. S. Ginger, *ACS Energy Lett.* **2016**, 1, 438–444; c) X. Yang, X. Zhang, J. Deng, Z. Chu, Q. Jiang, J. Meng, P. Wang, L. Zhang, Z. Yin, J. You, *Nat. Commun.* **2018**, 9, 570; d) Z. Fang, W. Chen, Y. Shi, J. Zhao, S. Chu, J. Zhang, Z. Xiao, *Adv. Funct. Mater.* **2020**, 30, 1909754.
- [20] Z. Xiao, R. A. Kerner, N. Tran, L. Zhao, G. D. Scholes, B. P. Rand, *Adv. Funct. Mater.* **2019**, 29, 1807284.
- [21] a) F. Wang, W. Geng, Y. Zhou, H.-H. Fang, C.-J. Tong, M. A. Loi, L.-M. Liu, N. Zhao, *Adv. Mater.* **2016**, 28, 9986–9992; b) D. H. Kim, C. P. Muzzillo, J. Tong, A. F. Palmstrom, B. W. Larson, C. Choi, S. P. Harvey, S. Glynn, J. B. Whitaker, F. Zhang, Z. Li, H. Lu, M. F. A. M. van Hest, J. J. Berry, L. M. Mansfield, Y. Huang, Y. Yan, K. Zhu, *Joule* **2019**, 3, 1734–1745; c) I. Zimmermann, S. Aghazada, M. K. Nazeeruddin, *Angew. Chem. Int. Ed.* **2019**, 58, 1072–1076; *Angew. Chem.* **2019**, 131, 1084–1088.
- [22] T. Zhou, H. Lai, T. Liu, D. Lu, X. Wan, X. Zhang, Y. Liu, Y. Chen, *Adv. Mater.* **2019**, 31, 1901242.
- [23] S. C. Rasmussen, S. J. Evenson, C. B. McCausland, *Chem. Commun.* **2015**, 51, 4528–4543.
- [24] M. Ban, Y. Zou, J. P. H. Rivett, Y. Yang, T. H. Thomas, Y. Tan, T. Song, X. Gao, D. Credginton, F. Deschler, H. Sirringhaus, B. Sun, *Nat. Commun.* **2018**, 9, 3892.
- [25] M. Zhang, F. Yuan, W. Zhao, B. Jiao, C. Ran, W. Zhang, Z. Wu, *Org. Electron.* **2018**, 60, 57–63.
- [26] A. Z. Chen, B. J. Foley, J. H. Ma, M. R. Alpert, J. S. Niezgodna, J. J. Choi, *J. Mater. Chem. A* **2017**, 5, 7796–7800.
- [27] J. Liu, L. Chen, B. Gao, X. Cao, Y. Han, Z. Xie, L. Wang, *J. Mater. Chem. A* **2013**, 1, 6216–6225.
- [28] a) T. Zhang, M. Long, M. Qin, X. Lu, S. Chen, F. Xie, L. Gong, J. Chen, M. Chu, Q. Miao, Z. Chen, W. Xu, P. Liu, W. Xie, J.-b. Xu, *Joule* **2018**, 2, 2706–2721; b) K. Liu, Q. Liang, M. Qin, D. Shen, H. Yin, Z. Ren, Y. Zhang, H. Zhang, P. W. K. Fong, Z. Wu, J. Huang, J. Hao, Z. Zheng, S. K. So, C.-S. Lee, X. Lu, G. Li, *Joule* **2020**, 4, 2404–2425.
- [29] A. Arakcheeva, D. Chernyshov, M. Spina, L. Forro, E. Horvath, *Acta Crystallogr. Sect. B* **2016**, 72, 716–722.
- [30] a) G. Kim, H. Min, K. S. Lee, D. Y. Lee, S. M. Yoon, S. I. Seok, *Science* **2020**, 370, 108–112; b) T. W. Jones, A. Osherov, M. Alsari, M. Sponseller, B. C. Duck, Y.-K. Jung, C. Settens, F. Niroui, R. Brenes, C. V. Stan, Y. Li, M. Abdi-Jalebi, N. Tamura, J. E. Macdonald, M. Burghammer, R. H. Friend, V. Bulović, A. Walsh, G. J. Wilson, S. Lilliu, S. D. Stranks, *Energy Environ. Sci.* **2019**, 12, 596–606.

Manuscript received: January 6, 2021

Accepted manuscript online: January 26, 2021

Version of record online: March 4, 2021